Journal of Drug Targeting

http://informahealthcare.com/drt
ISSN: 1061-186X (print), 1029-2330 (electronic)

J Drug Target, Early Online: 1–9
 DOI: 10.3109/1061186X.2014.928717

informa
healthcare

ORIGINAL ARTICLE

The effects of dendrimer size and central metal ions on photosensitizing properties of dendrimer porphyrins

Joo-Ho Kim, Hee-Jae Yoon, Jinsook Sim, Sang-Yong Ju, and Woo-Dong Jang

Department of Chemistry, Yonsei University, Seodaemun-Gu, Seoul, Korea

Abstract

A series of dendrimer porphyrins (G_nDP_M; n = generation of dendrimer, $n = 1–3$; M = coordination metal, M = freebase, Zn, Pt) were prepared and their photosensitizing properties were compared. All G_nDP_M exhibited sharp absorption in organic solvents. However, the Soret absorptions of $G_nDP_M(CO_2H)$ in 10 mM phosphate buffer solution (pH = 7.4) are broader than those of G_nDP_M in organic solvents, indicating inhomogeneous microenvironments of the focal porphyrin derivatives. All $G_3DP_M(CO_2H)$ successfully formed globular polyion complex micelles that were uniform in size. Under dark conditions, all $G_nDP_M(CO_2H)$ showed negligible cytotoxicity. However, all samples exhibited concentration-dependent photocytotoxicity under light irradiation. *In vitro* photocytotoxicity as well as singlet oxygen generation revealed that $G_3DP_{Zn}(CO_2H)$ is the best dendritic PS of the three different dendrimer porphyrin species.

Keywords

Copolymer, dendrimer, drug delivery, HeLa cells

History

Received 31 March 2014
Revised 18 May 2014
Accepted 22 May 2014
Published online 23 June 2014

Introduction

Photodynamic therapy (PDT) is a less-invasive therapeutic modality that utilizes nontoxic light-sensitive chemicals, photosensitizers (PSs), for the selective destruction of malignant tissue [1–3]. Unlike other types of phototherapy, PDT involves three key components: a PS, light and oxygen in the tissue. Light irradiation to the PS initiates a series of photochemical reactions that generate reactive oxygen species, which cause oxidative stress to the surrounding cells. Of the three key components, the most important is the design of effective PSs because it is not possible to fine tune light delivery conditions and oxygen concentrations in tumor tissue. Several parameters must be considered for the design of effective PSs. First, PSs should be basically nontoxic but become highly toxic under light irradiation. To achieve such high photocytotoxicity, PSs require large absorption cross-sections with high quantum yield for singlet oxygen ($^1O_2$) production [4–6]. The most common conventional PSs are composed of porphyrin derivatives that have a strong extinction coefficient with visible light absorption due to expanded π-conjugation domains [7,8]. Although expanded π-conjugation domains are useful for effective light absorption, the skeletons of porphyrin moieties are basically hydrophobic and easily form aggregates in aqueous media due to strong π–π interactions as well as their hydrophobic nature. Therefore, the efficacy of some PSs decreases in high local concentrations. Several years ago, we developed dendritic PSs to overcome this drawback [9–12]. The large dendritic wages can effectively segregate focal PS units from external environments and improve solubility in aqueous media. The charged periphery of dendritic PSs can associate with oppositely charged hydrophilic block copolymers to form polyion complex (PIC) micelles [9,11]. Initial studies of dendritic PSs were focused on the evaluation of effectiveness in a variety of animal models [13,14]. Then studies moved on to the application of dendritic PSs for drug or nucleic acid delivery. Several formulations have been designed for the light-driven delivery of drugs and nucleic acids [15–20]. Based on these results, we are currently preparing new types of nanodevices for the combination of PDT by dendritic PSs and other therapeutics or diagnostic tools [21–23]. Along these lines, we have assessed the effectiveness of dendritic PSs and the structural utility of dendritic architecture [14,21–26]. However, the effective PDT effects of dendritic PSs remain incompletely understood.

In this study, we investigate the effects of the sizes of dendritic wedges and central metal ions on photosensitizing properties. A series of dendrimer porphyrins (G_nDP_M; n = generation of dendrimer, $n = 1–3$; M = coordination metal, M = freebase (FB), Zn, Pt; Figure 1) were prepared and their photosensitizing properties were compared.

Materials and methods

Materials

Chemicals for dendrimer and polymer syntheses were purchased from Tokyo Kasei Co., Ltd. (Tokyo, Japan) and

Address for correspondence: Professor Woo-Dong Jang, Department of Chemistry, Yonsei University, Seoul, Republic of Korea. E-mail: wdjang@yonsei.ac.kr

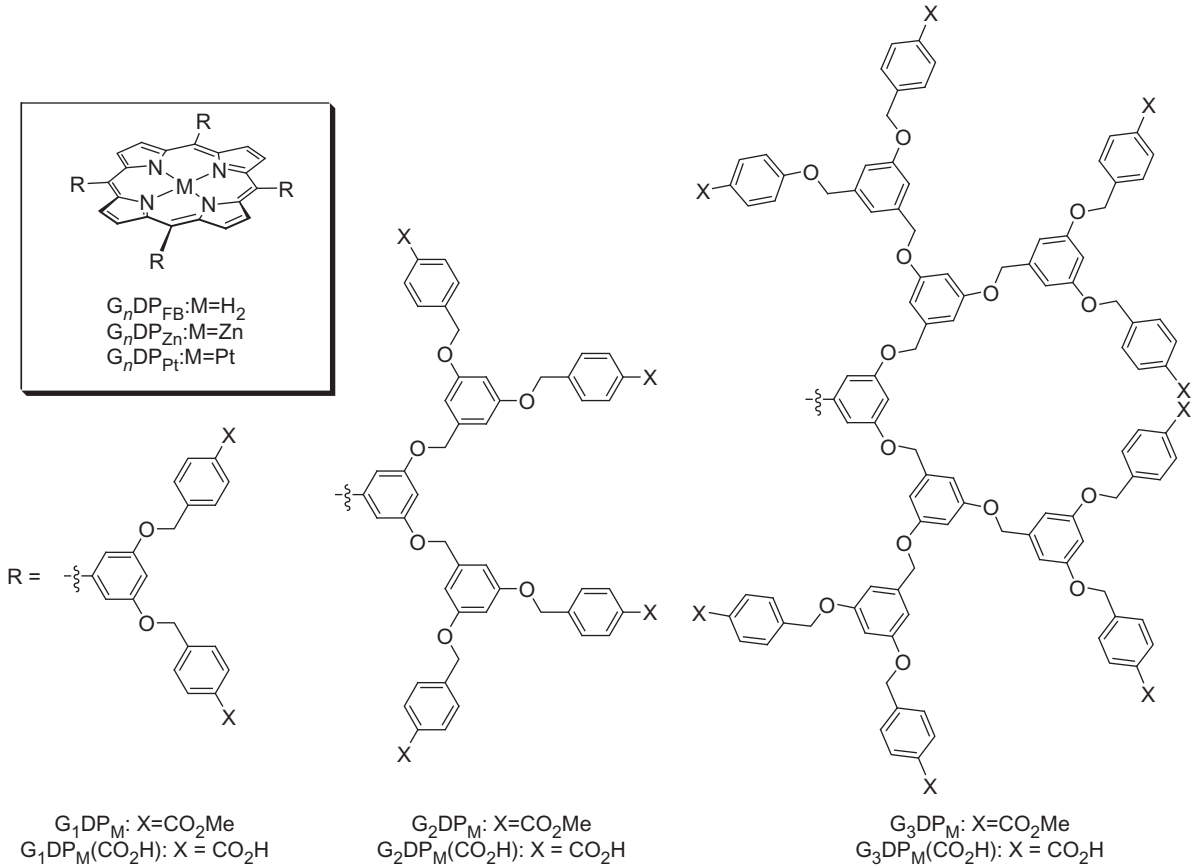

Figure 1. Structures of dendrimer porphyrins.

Sigma-Aldrich Co., Inc. (St Louis, MO) and used without further purification. All solvents for dendrimer and polymer syntheses were freshly distilled just before use. α-Methoxy-ϖ-amino-poly(ethylene glycol) (MeO–PEG–NH_2, MW = 12 kg/mol) was purchased for block copolymer synthesis from Nippon Oil and Fats, Co., Ltd (Tokyo, Japan).

Synthesis

G_nDP_M was prepared following previously reported procedures [12,27]. Briefly, alkali-mediated coupling of 5, 10, 15, 20-tetrakis (3′,5′-dihydroxyphenyl)porphyrin with methoxycarbonyl-terminated poly(benzyl ether) dendritic bromides was carried out to obtain G_nDP_{FB}. G_nDP_{Zn} was obtained by subjecting G_nDP_{FB} to a simple metalation process by the treatment of $Zn(OAc)_2$ in $MeOH/CH_2Cl_2$. Because the introduction of Pt(II) to the porphyrin center requires very harsh conditions, Pt(II)-coordinated porphyrin (P_{Pt}-OMe) was prepared and methoxy groups were converted into hydroxyl groups by the treatment of BBr_3 in CH_2Cl_2. Then, poly(benzyl ether) dendritic bromides were introduced to the hydroxyl groups to obtain G_nDP_{Pt}. Finally, surface methoxycarbonyl groups were hydrolyzed to obtain water-soluble forms of G_nDP_M ($G_nDP_M(CO_2H)$). The synthesis of G_nDP_{Pt} was conducted as follows (Scheme 1):

P_{Pt}-OMe: P_{FB}-OMe (200 mg, 0.233 mmol) and $PtCl_2$(II) (185 mg, 0.699 mmol) was dissolved in dried benzonitrile (10 mL) and refluxed for 10 h under N_2 atmosphere. The solvent was removed *in vacuo*, and the residue was purified with silica column chromatography. The recrystallized form CH_2Cl_2/hexane, P_{Pt}-OMe, was obtained as an orange solid with a 36% yield (244 mg). ^{1}H NMR (400 MHz, $CDCl_3$): δ 4.02 (s, 24 H, OCH_3), 7.21 (s, 4 H, *p*-H C_6H_3), 7.33 (s, 8 H, *o*-H C_6H_3) and 8.83 (s, 8 H, pyrrole-β-H).

P_{Pt}-OH: BBr_3 (1.9 mL, 1.0 M in CH_2Cl_2) was slowly added to a CH_2Cl_2 (40 mL) solution of P_{Pt}-OMe (200 mg, 0.19 mmol) and stirred for 2 h at 0 °C. The reaction mixture was quenched with H_2O (10 mL) and poured into saturated aqueous $NaHCO_3$ solution, which was extracted with EtOAc. The combined organic layer was dried over anhydrous $MgSO_4$ and evaporated. The residue was recrystallized (MeOH/CH_2Cl_2) to obtain P_{Pt}-OH as an orange solid (140 mg, 80%). ^{1}H NMR (400 MHz, dimethylsulfoxide (DMSO)-d_6): δ 6.64 (s, 4 H; *p*-H C_6H_3), 6.95 (s, 8 H; *o*-H C_6H_3), 8.84 (s, 8 H; pyrrole-β-H) and 9.71 (s, 8 H, OH).

G_1DP_{Pt}: To a tetrahydrofuran (THF) (10 mL) solution of P_{Pt}-OH (50 mg, 0.053 mmol) and methyl-4-bromomethylbenzoate (121 mg, 0.53 mmol), K_2CO_3 (22 mg, 0.16 mmol) and 18-crown-6 (14 mg) were added and refluxed for 24 h. The reaction mixture was evaporated to dryness, and the residue was purified with silica column chromatography to obtain G_1DP_{Pt} as an orange solid (80 mg, 71%). ^{1}H NMR (400 MHz, $CDCl_3$): δ 3.89 (s, 24 H; CO_2CH_3), 5.27 (s, 16 H; O-CH_2), 7.03 (s, 4 H; *p*-H C_6H_3), 7.40 (s, 8 H; *o*-H C_6H_3), 7.56 (d, 16 H; *o*-H C_6H_4), 8.07 (d, 16 H; *m*-H C_6H_4) and 8.72 (s, 8 H; pyrrole-β-H). matrix-assisted laser desorption ionization time-of-flight mass-spectroscopy (MALDI-TOF-MS): m/z = 2121.141.

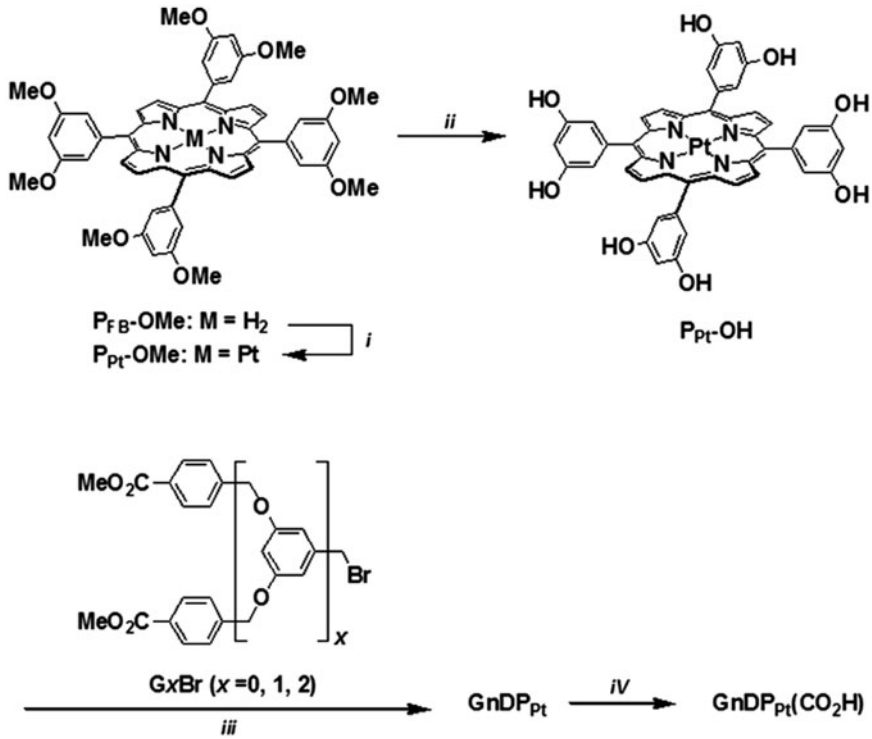

Scheme 1. Synthetic route of G_nDP_{Pt}. (i) $PtCl_2$, benzonitrile, reflux, 10 h; (ii) BBr_3, CH_2Cl_2, –78 °C, 1 h; (iii) G_xBr ($x = 0$, 1, 2), K_2CO_3, 18-crown-6, THF, reflux, 24 h; and (iv) 3 M NaOH(aq), H_2O/THF, reflux, 20 h.

G_2DP_{Pt}: To a THF (10 mL) solution of P_{Pt}-OH (50 mg, 0.053 mmol) and G1Br (265 mg, 0.53 mmol), K_2CO_3 (22 mg, 0.16 mmol) and 18-crown-6 (14 mg) were added and refluxed for 24 h. The reaction mixture was evaporated to dryness, and the residue was purified with silica column chromatography to obtain G_2DP_{Pt} as an orange solid (160 mg, 70%). ^{1}H NMR (400 MHz, $CDCl_3$): δ 3.85 (s, 48 H; CO_2CH_3), 4.97 (s, 32 H; O-CH_2), 5.10 (s, 32 H; O-CH_2), 6.53 (s, 8 H; *p*-H C_6H_3), 6.70 (s, 16 H; *o*-H outer C_6H_3), 7.00 (s, 4 H; *p*-H inner C_6H_3), 7.32 (d, 32 H; *o*-H C_6H_4), 7.35 (s, 8 H; *o*-H inner C_6H_3), 7.90 (d, 32 H; *m*-H C_6H_4) and 8.71 (s, 8 H; pyrrole-β-H). MALDI-TOF-MS: m/z = 4284.783.

G_3DP_{Pt}: To a THF (8 mL) solution of P_{Pt}-OH (46 mg, 0.049 mmol) and G1Br (509 mg, 0.49 mmol), K_2CO_3 (7 mg, 0.05 mmol) and 18-crown-6 (5 mg) were added and refluxed for 24 h. The reaction mixture was evaporated to dryness, and the residue was purified with silica column chromatography to obtain G_3DP_{Pt} as an orange solid (300 mg, 71%). ^{1}H NMR (400 MHz, $CDCl_3$): δ 3.81 (s, 96 H; CO_2CH_3), 4.83 (s, 64 H; outer O-CH_2), 4.87 (s, 32 H; mid O-CH_2), 5.05 (s, 16 H; inner O-CH_2), 6.38 (s, 16H; *o*-H mid C_6H_3), 6.51 (s, 32H; *o*-H outer C_6H_3), 6.67(s, 16H; *p*-H outer C_6H_3), 7.00 (s, 4H, *p*-H inner C_6H_3), 7.25 (d, 64 H; *p*-H inner C_6H_4), 7.37 (s, 8 H; *o*-H inner C_6H_3), 7.81 (s, 8 H, *p*-H mid C_6H_3), 7.89 (d, 64 H; *m*-H C_6H_4) and 8.76 (s, 8 H; pyrrole-β-H). MALDI-TOF-MS: m/z = 8615.107.

$G_3DP_{Pt}(CO_2H)$: To a THF (10 mL) solution of G_3DP_{Pt}, 3 M NaOH(aq) (10 mL) was added and refluxed for 20 h. The solution was dialyzed with pure water using a 1000 g/mol cut-off dialysis membrane for two days and freeze-dried to obtain $G_3DP_{Pt}(CO_2H)$.

Poly(ethylene glycol)-*block*-poly(L-lysine) (PEG-*b*-PLL) was synthesized by the polymerization of N-carboxyanhydride of N^{ε}-Z-L-lysine initiated by CH_3O-PEG-NH_2 (12 000 g/mol) in DMF, followed by deprotection of the Z group according to a previously reported method [12]. The degree of polymerization of PLL was determined to be 40 by gel-permeation chromatography and ^{1}H NMR spectroscopy, respectively.

Formation of PIC micelle

The PIC micelles were prepared by mixing $G_3DP_M(CO_2H)$ and PEG-*b*-PLL at a stoichiometric charge ratio. In a typical procedure, PEG-*b*-PLL (2.8 mg) was dissolved in a 10 mM NaH_2PO_4 solution (1.23 mL) and added to $G_3DP_M(CO_2H)$ (1.2 mg) in a 10 mM Na_2HPO_4 solution (2.77 mL) to obtain a solution containing $G_3DP_M(CO_2H)$ incorporated PIC micelles in a 10 mM phosphate buffered solution (pH 7.4).

Octanol/water partitioning

$G_nDP_{Pt}(CO_2H)$ (10 μM) in 25 mM phosphate buffer solution (PBS; 3 mL) containing 150 mM NaCl with varying pH (4.5–8.0) was mixed with the same volume of 1-octanol. The mixture was vigorously shaken by a vortex mixer. The amount of $G_nDP_{Pt}(CO_2H)$ remaining in the aqueous phase was determined from the decrease in the Soret absorption band to calculate the octanol/water partitioning ratio of $G_nDP_{Pt}(CO_2H)$.

Measurements

The UV/Vis absorptions of each dendrimer were measured by a JASCO V-660 spectrophotometer (JASCO, Tokyo, Japan) in various solvents, including THF, toluene, DMSO and H_2O. The dynamic light scattering of PIC micelle was measured using a Zetasizer nano ZS (Malvern, Worcestershire, UK). The morphologies of PIC micelles were assessed using field emission scanning electron microscopy (FE-SEM). FE-SEM was performed with a JEOL Model JSM-6701F at 30 kV

(JEOL Ltd., Tokyo, Japan). ^{1}H spectra were obtained on a Bruker DPX-400(400 MHz) spectrometer (Billerica, MA). MALDI-TOF-MS measurements were performed on a Bruker model LRF20 using dithranol as a matrix. The steady-state luminescence of $^1O_2$ was directly observed around 1275 nm using a Spex Nanolog 3-211 spectrofluorometer (HORIBA, Kyoto, Japan) upon excitation of the Soret band of each dendrimer. $^1O_2$ detection in PBS was carried out using singlet oxygen sensor green (SOSG) (Molecular Probes, Inc., Eugene, OR). To $G_nDP_M(CO_2H)$ (1.0 μM, 2 mL) in 10 mM PBS containing 150 mM NaCl, MeOH solution of SOSG (1 mM, 10 μL) was added. Then, the mixture solution was photoirradiated for 30 min with a broad-band visible light from a light emitting diode (LED; incident energy 66 kJ cm^{-2}). Finally, the fluorescence intensity of SOSG was measured.

Cell experiments

HeLa cells were used to evaluate the PDT effects of each dendrimer *in vitro*. Cells were maintained as a monolayer in RPMI 1640 containing 10% fetal bovine serum and 1% antibiotics in a humidified atmosphere containing 5% CO_2 at 37 °C. For the cytotoxicity assay, the cells were photoirradiated for 1 h with broad-band visible light from a LED (incident energy 132 kJ cm^{-2}). The viability of the cells was evaluated by the 3-(4,5-dimethylthiazol-2-yl)-2,5-diphenyltetrazolium bromide (MTT) assay. All dendrimer samples were first dissolved in 10 mM Na_2HPO_4 solution, and the pH of the solution was set to 7.4 by adding 10 mM NaH_2PO_4 solution. The concentration of prepared DP stock solution was 10^{-4} M. For treatment, the stock solutions were diluted with culture medium (1/5 dilution), which is of the highest concentration (2 μM). For each sample, 10 cases with different concentrations (1/2 dilution) were tested.

Results and discussion

G_nDP_{FB} and G_nDP_{Zn} were prepared based on a previously reported procedure [27]. For the synthesis of G_nDP_{Pt}, Pt(II)-coordinated porphyrin (P_{Pt}-OH) was newly synthesized and reacted with G_nBr to obtain G_nDP_{Pt}. All G_nDP_M were hydrolyzed by treatment with 3 M NaOH to obtain water-soluble $G_nDP_M(CO_2H)$. All G_nDP_M were unambiguously characterized by ^{1}H NMR and MALDI-TOF-MS analyses. All G_nDP_M exhibited very high solubility in several organic solvents, including toluene, THF and DMSO. The hydrolyzed form of G_nDP_M, $G_nDP_M(CO_2H)$, also exhibited very high solubility in aqueous media due to the ionic charges of the dendritic wedges. UV/Vis absorption spectra of G_nDP_M and $G_nDP_M(CO_2H)$ were measured in various solvents (10.0 μM) (Figure 2). The wavelengths of absorption maxima and full width of half maximum (FWHM) values at the Soret band are summarized in Table 1. All G_nDP_M exhibited sharp absorption bands in organic solvents. However, the Soret absorptions of $G_nDP_M(CO_2H)$ in 10 mM PBS (pH = 7.4) became broader than those of G_nDP_M in organic solvents, indicating inhomogeneous microenvironments of the focal porphyrin derivatives. Because THF, toluene and DMSO are good solvents for both dendritic wedge and core porphyrin derivatives, the dendritic wedges in all G_nDP_M may have fully extended conformations. Therefore, the core porphyrin derivatives would directly contact solvent molecules. In fact, all G_nDP_M exhibits similar FWHM values within the same metalloporphyrin series. In contrast, high solubility of $G_nDP_M(CO_2H)$ in PBS can be achieved by the carboxylate groups on the periphery. The dendritic building blocks as well as the porphyrin core have basically hydrophobic natures. Therefore, dendritic wedges will not adopt fully extended conformations in PBS to reduce the exposure of their hydrophobic skeletons or the focal porphyrin structure to the aqueous phase [28–30]. Moreover, the relatively open architecture of low generation dendrimers may induce self-aggregation. In fact, $G_1DP_M(CO_2H)$ have absorption maxima at the more highly blue-shifted region than those of $G_2DP_M(CO_2H)$ or $G_3DP_M(CO_2H)$, indicating the formation of H-aggregates in the aqueous phase. Figure 3(a) shows normalized absorption spectra of $G_1DP_{Zn}(CO_2H)$ upon dilution in PBS. According to the increasing concentration, the intensity of the peak at 402 nm was gradually increased by the formation of H-aggregates. In contrast, the absorption maximum of $G_3DP_M(CO_2H)$ appeared in the longest wavelength region. The absorption spectrum of $G_3DP_{Zn}(CO_2H)$ in PBS lacks concentration dependency, indicating that large dendritic wedges can effectively prevent aggregation (Figure 3b).

$G_3DP_M(CO_2H)$ can form supramolecular PIC micelles by mixing with PEG-*b*-PLL in a stoichiometric ratio of positive and negative charges [9,11]. When solutions of $G_3DP_M(CO_2H)$ in 10 mM Na_2HPO_4 solution were mixed with PEG-*b*-PLL in 10 mM NaH_2PO_4 solution, all $G_3DP_M(CO_2H)$ successfully formed globular PIC micelles that were uniform in size. The formation of PIC micelles was confirmed by FE-SEM (Figure 4). All PIC micelles exhibited the same morphologies, indicating that $G_3DP_M(CO_2H)$ have similar solution behaviors regardless of central metal coordination due to large dendritic wedge substitution.

PDT effects against HeLa cells were evaluated *in vitro* for all $G_nDP_M(CO_2H)$ by MTT assay. Under dark conditions, all $G_nDP_M(CO_2H)$ showed negligible cytotoxicity. However, all samples exhibited concentration-dependent photocytotoxicity under light irradiation. Due to the increasing dendrimer size, all series of $G_nDP_M(CO_2H)$ tend to increase photocytotoxicity. Platinum-coordinated porphyrin derivatives are known to be efficient $^1O_2$ generators due to the high intersystem crossing quantum yield achieved by heavy-atom effects [31–37]. However, within three different series of porphyrin dendrimers, $G_nDP_{Zn}(CO_2H)$ exhibited the highest photocytotoxicity but $G_nDP_{FB}(CO_2H)$ and $G_nDP_{Pt}(CO_2H)$ exhibited very similar PDT effects (Figure 5).

Based on the above information, we attempted direct observation of photoluminescence from $^1O_2$ in various solvents. Fixed concentrations (1.0 μM) of G_nDP_M and $G_nDP_M(CO_2H)$ solutions in several organic solvents and PBS were prepared for the evaluation of $^1O_2$ detection. Upon the excitation of Soret bands of each solution, the relative intensities of photoluminescence around 1275 nm were recorded. The intensity of photoluminescence from $^1O_2$ was dependent on the polarity of solvents. By changing from nonpolar solvents to polar solvents, the intensity of photoluminescence gradually decreased as shown in Figure 6. Typically, the intensity of $^1O_2$ photoluminescence in PBS was

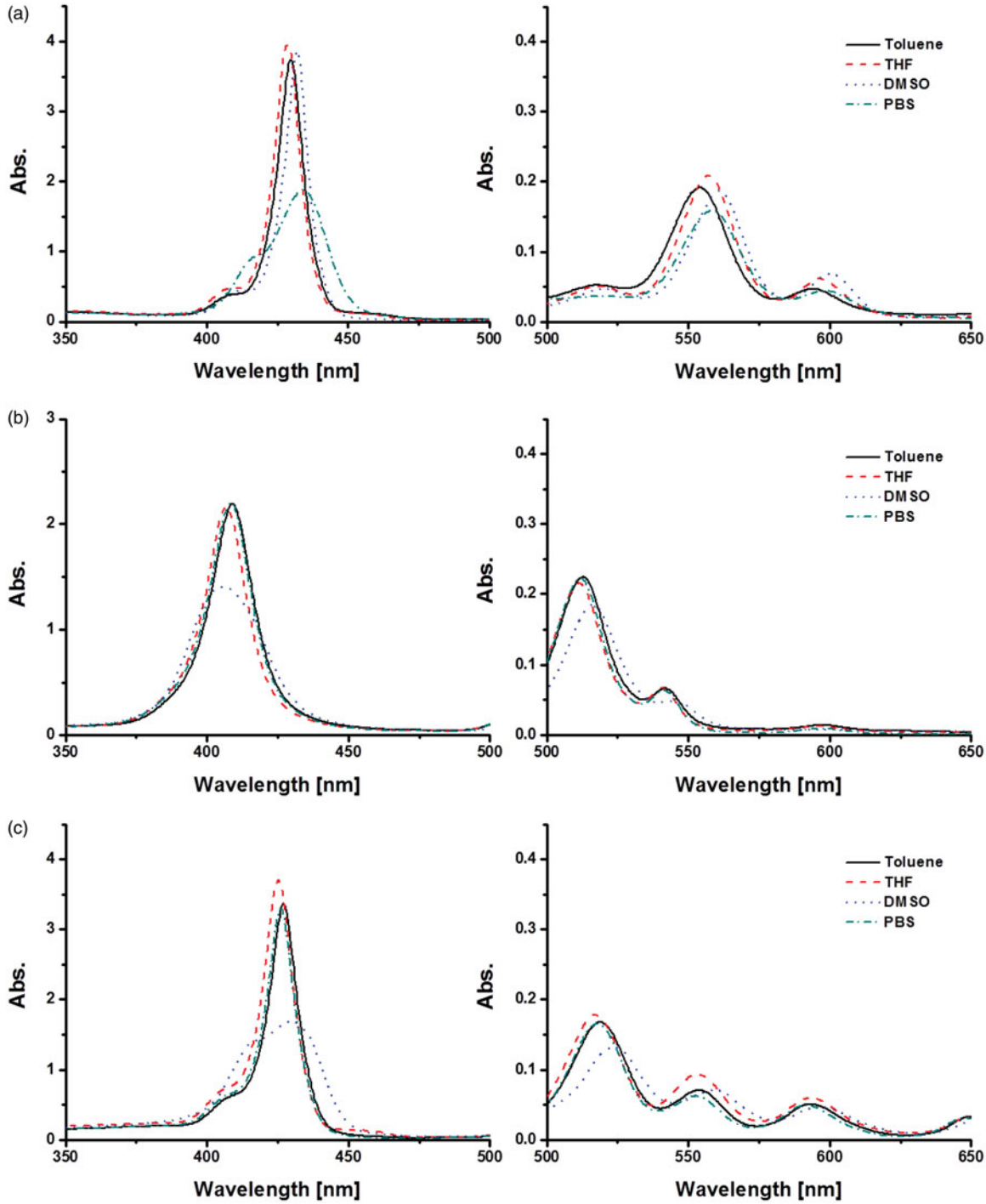

Figure 2. UV/Vis absorption spectra of G_3DP_M and $G_3DP_M(CO_2H)$ in various organic solvents and pH 7.4 PBS (10 μM). (a) G_3DP_{Zn} and $G_3DP_{Zn}(CO_2H)$, (b) G_3DP_{Pt} and $G_3DP_{Pt}(CO_2H)$, and (c) G_3DP_{FB} and $G_3DP_{FB}(CO_2H)$.

significantly weaker than in organic solvents. Such aspects can be explained by poor $^1O_2$ quantum yield as well as the reduced lifetime of $^1O_2$ in aqueous media. In fact, the lifetime of $^1O_2$ in aqueous media is 1/100 of that in THF [38]. Although we compared the photoluminescence intensities of $^1O_2$ in aqueous media, we were unable to obtain reliable data for $^1O_2$ generation in aqueous media due to the weak signal intensity. Therefore, we utilized the indirect method. The generation efficacy of $^1O_2$ of $G_nDP_M(CO_2H)$ in PBS was compared using SOSG. First, we compared the $^1O_2$ generation ability of different generations of G_nDP_M in the same metal series in THF. In the cell viability test, larger dendrimers exhibited higher photocytotoxicity for all series of dendrimers. However, the production of $^1O_2$ in the same solvents was comparable in the same metal series of dendrimers regardless of generation, indicating that the higher toxicity of larger dendrimers did not cause differences in $^1O_2$ generation quantum yield. In contrast, G_nDP_{Zn} exhibited the highest $^1O_2$ generation ability in comparisons with different metal series, which is consistent with the photocytotoxicity evaluation. Therefore, we can conclude that the highest photocytotoxicity of $G_nDP_{Zn}(CO_2H)$ within three different metal series originated from the highest $^1O_2$ generation efficiency. However, the generation dependency

of photocytotoxicity cannot be explained by $^1O_2$ generation efficiency in THF. The results of the $^1O_2$ detection experiment using SOSG in PBS indicated slightly higher $^1O_2$ generation efficacy for larger dendrimers (Figure 7).

In a previous investigation, we found that larger dendrimers exhibited slightly higher cellular uptake within the $G_nDP_{Zn}(CO_2H)$ series [12]. However, the differences in the cellular uptake amounts were within error ranges. Therefore, the generation dependency of photocytotoxicity cannot be fully explained by cellular uptake or $^1O_2$ generation efficiency. We hypothesize two different mechanisms for the explanation of generation dependency in photocytotoxicity. One is based on the ease of aggregation of small dendrimers. When dendrimer uptake occurs by endocytosis, surface carboxylates are protonated by decreases of pH, and $G_nDP_M(CO_2H)$ becomes hydrophobic. In such conditions, small $G_nDP_M(CO_2H)$ easily forms aggregates. The results of octanol/water partitioning experiments indicate that the solubility of $G_1DP_M(CO_2H)$ can be greatly decreased by pH lowering (Figure 8). The partitioning of $G_1DP_{Pt}(CO_2H)$ to the aqueous phase significantly decreased as pH decreased from 7.0 to 6.5. In contrast, large dendrimers can effectively prevent the aggregation of porphyrin cores when they become insoluble in acidic conditions. Compared to $G_1DP_{Pt}(CO_2H)$, $G_2DP_{Pt}(CO_2H)$ and $G_3DP_{Pt}(CO_2H)$ exhibited improved solubility at pH 5.0 to 6.5. The cell viability curve of the $G_nDP_{Zn}(CO_2H)$ series shows that the photocytotoxicity of $G_1DP_{Zn}(CO_2H)$ is slightly higher than that of $G_2DP_{Zn}(CO_2H)$ at low concentrations. As concentrations increase, the photocytotoxicity of $G_2DP_{Zn}(CO_2H)$ becomes greater than that of $G_1DP_{Zn}(CO_2H)$. This might be due to the formation of aggregates of $G_1DP_{Zn}(CO_2H)$ at high concentrations. The second hypothesis considers the improved $^1O_2$ generation quantum yield of porphyrin cores in hydrophobically protected dendrimer cores. Because small dendrimers have relatively open architecture, the core porphyrin is exposed

Table 1. The wavelengths of absorption maxima and full width of half maximum (FWHM) values G_nDP_M.

	Toluene (λmax*/FWHM†)	DMSO	THF	PBS (pH 7.4)‡
G_1DP_{FB}	423/643	423/648	420/673	406/2309
G_1DP_{Zn}	427/570	430/459	426/510	404/2066
G_1DP_{Pt}	405/1013	406/1047	403/1076	385/1449
G_2DP_{FB}	424/633	424/652	422/690	415/1921
G_2DP_{Zn}	428/577	431/510	427/593	432/1733
G_2DP_{Pt}	407/1045	407/1091	405/1147	406/1835
G_3DP_{FB}	427/600	426/669	425/707	429/1895
G_3DP_{Zn}	430/959	432/533	429/595	434/1294
G_3DP_{Pt}	409/1079	408/1096	407/1063	412/1851

*nm, †cm^{-1}, ‡$G_nDP_M(CO_2H)$ used and PBS contains 150 mM NaCl.

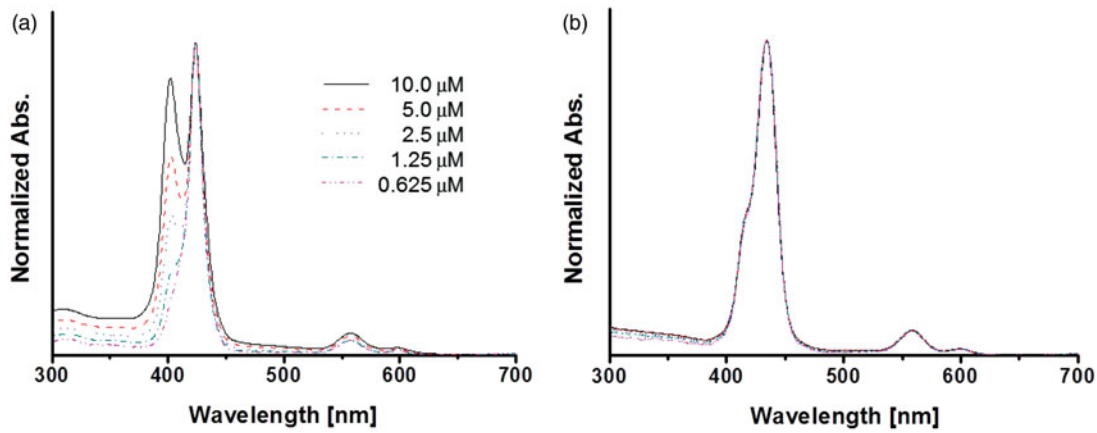

Figure 3. Normalized UV/Vis absorption spectra of (a) $G_1DP_{Zn}(CO_2H)$ and (b) $G_3DP_{Zn}(CO_2H)$ upon dilution in pH 7.4 PBS (10, 5, 2.5, 1.25 and 0.625 μM).

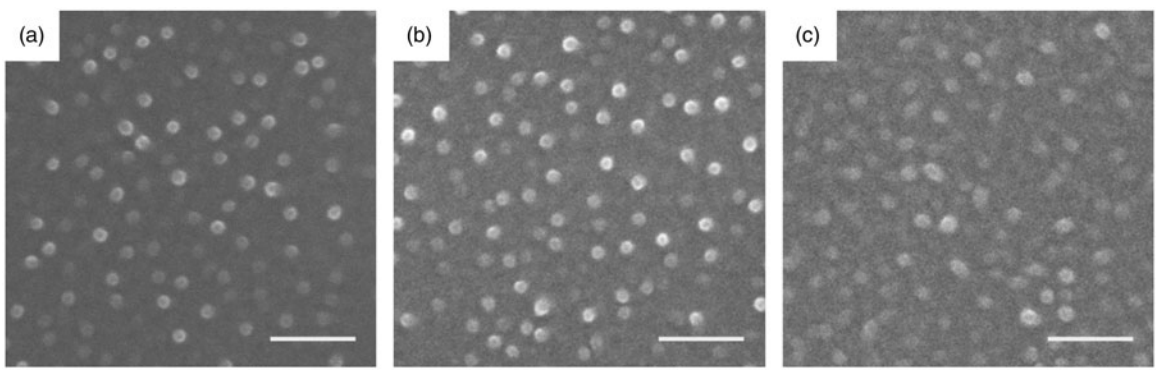

Figure 4. FE-SEM images of polyion complex micelles with PEG-*b*-PLL and $G_3DP_M(CO_2H)$. (a) $G_3DP_{FB}(CO_2H)$, (b) $G_3DP_{Zn}(CO_2H)$ and (c) $G_3DP_{Pt}(CO_2H)$. (Scale bar = 100 nm).

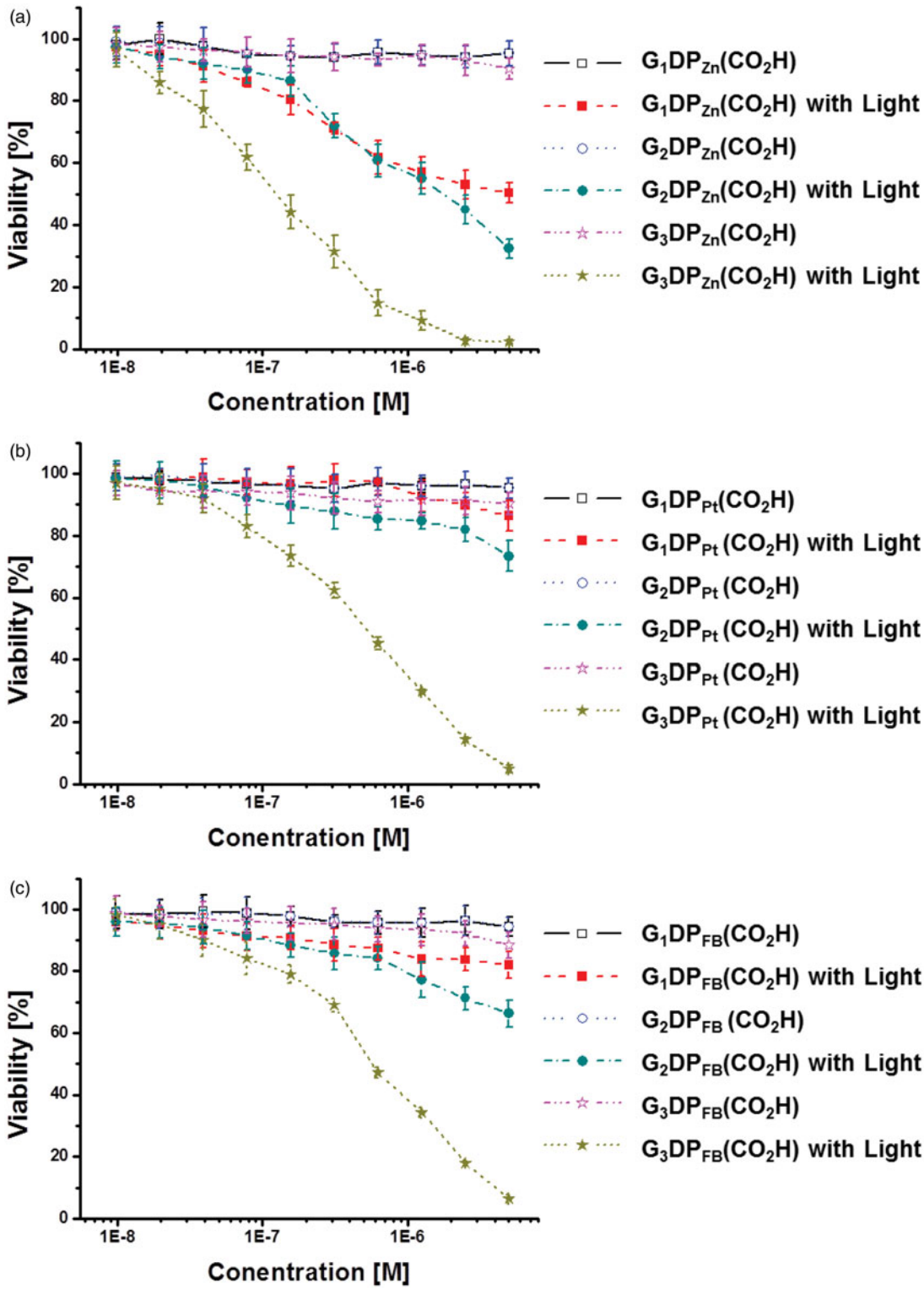

Figure 5. Cell viability curves of (a) $G_nDP_{Zn}(CO_2H)$, (b) $G_nDP_{Pt}(CO_2H)$ and (c) $G_nDP_{FB}(CO_2H)$. Error bars indicate standard deviation, $n = 4$.

to hydrophilic environments. In contrast, large dendrimers may prevent the access of polar solvent molecules to focal porphyrin units, typically in acidic conditions, in endosomes because the protonation of surface carboxylates causes shrinkage of dendritic wedges. In fact, the results of $^1O_2$ detection experiments using SOSG in PBS indicated the higher $^1O_2$ generation efficacy of larger dendrimers.

In conclusion, we synthesized three different series of dendritic PSs to investigate the effects of central metal ions and dendrimer size on photosensitizing properties. Within three different porphyrin species, Zn(II) coordinated porphyrins exhibited the highest photocytotoxicity as well as $^1O_2$ generation efficiency in THF. In the cell viability assay, larger generation dendrimers exhibited higher photocytotoxicity for the entire range of $G_nDP_m(CO_2H)$. $G_3DP_{Zn}(CO_2H)$ is the best choice for a dendritic PS involving a large dendritic wedge and a central metal ion. Although we continuously carried out PDT-related experiments using $G_3DP_{Zn}(CO_2H)$ as

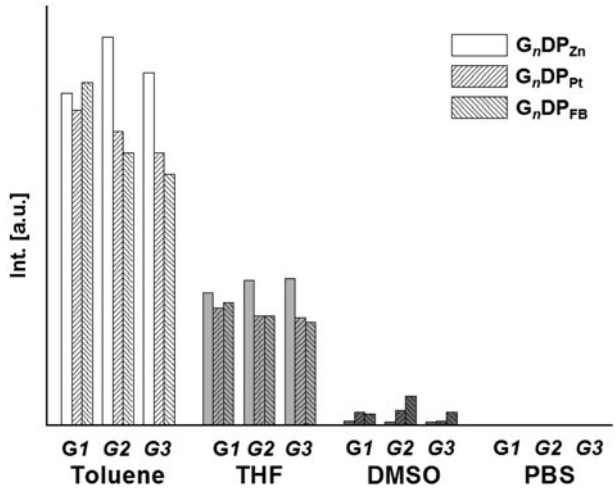

Figure 6. Photoluminescence intensities of G_nDP_M (1 μM) at 1275 nm in various solvents.

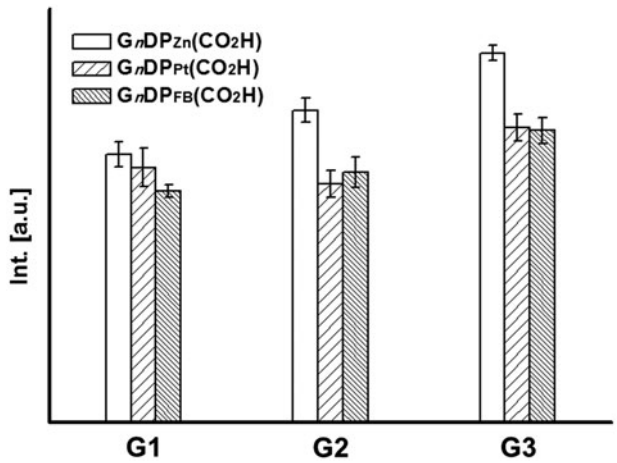

Figure 7. Detection of singlet oxygen using SOSG in $G_nDP_M(CO_2H)$ (1.0 μM) solutions.

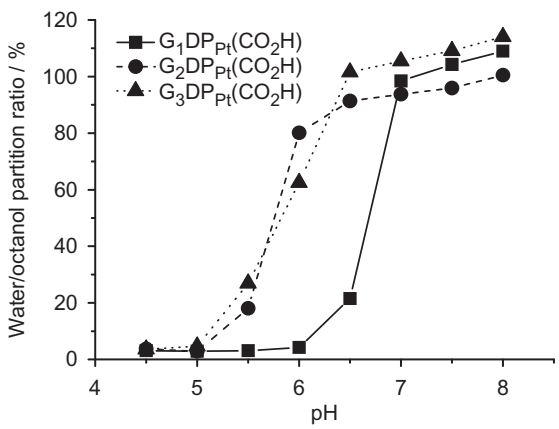

Figure 8. Octanol/water partition ratios of $G_nDP_{Pt}(CO_2H)$ in various pH.

the dendritic PS, the exact mechanism explaining the improved PDT efficacy remains unclear. This research is an important starting point for the understanding of mechanisms underlying the improved PDT efficacy of dendritic PS.

Acknowledgements

The authors wish to express their sincere thanks to Professor Kazunori Kataoka of the University of Tokyo for his support of this work.

Declaration of interest

This work was supported by the Mid-Career Researcher Program (No. 2012005565) funded by the National Research Foundation (NRF) under the Ministry of Science, ICT & Future, Korea.

References

1. Dougherty TJ, Gomer CJ, Henderson BW, et al. Photodynamic therapy. J Natl Cancer Inst 1998;90:889–905.
2. Dolmans DE, Fukumura D, Jain RK. Photodynamic therapy for cancer. Nature reviews. Cancer 2003;3:380–7.
3. Henderson BW, Dougherty TJ. How does photodynamic therapy work? Photochem Photobiol 1992;55:145–57.
4. Derycke AS, de Witte PA. Liposomes for photodynamic therapy. Adv Drug Deliv Rev 2004;56:17–30.
5. van Dongen GA, Visser GW, Vrouenraets MB. Photosensitizer-antibody conjugates for detection and therapy of cancer. Adv Drug Deliv Rev 2004;56:31–52.
6. Gerhardt SA, Lewis JW, Kliger DS, et al. Effect of micelles on oxygen-quenching processes of triplet-state para-substituted tetraphenylporphyrin photosensitizers. J Phys Chem A 2003;107:2763–7.
7. Bonnett R. Photosensitizers of the porphyrin and phthalocyanine series for photodynamic therapy. Chem Soc Rev 1995;24:19–33.
8. O'Connor AE, Gallagher WM, Byrne AT. Porphyrin and nonporphyrin photosensitizers in oncology: preclinical and clinical advances in photodynamic therapy. Photochem Photobiol 2009;85:1053–74.
9. Jang W-D, Nishiyama N, Zhang G-D, et al. Supramolecular nanocarrier of anionic dendrimer porphyrins with cationic block copolymers modified with polyethylene glycol to enhance intracellular photodynamic efficacy. Angew Chem Int Ed 2005;44:419–23.
10. Nishiyama N, Stapert HR, Zhang GD, et al. Light-harvesting ionic dendrimer porphyrins as new photosensitizers for photodynamic therapy. Bioconjugate Chem 2003;14:58–66.
11. Jang W-D, Nakagishi Y, Nishiyama N, et al. Polyion complex micelles for photodynamic therapy: incorporation of dendritic photosensitizer excitable at long wavelength relevant to improved tissue-penetrating property. J Control Release 2006;113:73–9.
12. Li Y, Jang W-D, Nishiyama N, et al. Dendrimer generation effects on photodynamic efficacy of dendrimer porphyrins and dendrimer-loaded supramolecular nanocarriers. Chem Mater 2007;19:5557–62.
13. Nishiyama N, Nakagishi Y, Morimoto Y, et al. Enhanced photodynamic cancer treatment by supramolecular nanocarriers charged with dendrimer phthalocyanine. J Controlled Release 2009;133:245–51.
14. Ideta R, Tasaka F, Jang W-D, et al. Nanotechnology-based photodynamic therapy for neovascular disease using a supramolecular nanocarrier loaded with a dendritic photosensitizer. Nano Lett 2005;5:2426–31.
15. Delcea M, Mohwald H, Skirtach AG. Stimuli-responsive LbL capsules and nanoshells for drug delivery. Adv Drug Deliv Rev 2011;63:730–47.
16. Barhoumi A, Huschka R, Bardhan R, et al. Light-induced release of DNA from plasmon-resonant nanoparticles: towards light-controlled gene therapy. Chem Phys Lett 2009;482:171–9.
17. Erokhina S, Benassi L, Bianchini P, et al. Light-driven release from polymeric microcapsules functionalized with bacteriorhodopsin. J Am Chem Soc 2009;131:9800–4.
18. Bédard M, Skirtach AG, Sukhorukov G. Optically driven encapsulation using novel polymeric hollow shells containing an azobenzene polymer. Macromol Rapid Commun 2007;28:1517–21.
19. Cotí KK, Belowich ME, Liong M, et al. Mechanised nanoparticles for drug delivery. Nanoscale 2009;1:16–39.

20. Lu J, Choi E, Tamanoi F, Zink JI. Light-activated nanoimpeller-controlled drug release in cancer cells. Small 2008;4:421–6.
21. Yoon H-J, Lim TG, Kim J-H, et al. Fabrication of multifunctional layer-by-layer nanocapsules toward the design of theragnostic nanoplatform. Biomacromolecules 2014;15:1382–9.
22. Son KJ, Yoon H-J, Kim J-H, et al. Photosensitizing hollow nanocapsules for combination cancer therapy. Angew Chem Int Ed 2011;50:11968–71.
23. Kim J, Yoon H-J, Kim S, et al. Polymer–metal complex micelles for the combination of sustained drug releasing and photodynamic therapy. J Mater Chem 2009;19:4627–31.
24. Nishiyama N, Iriyama A, Jang W-D, et al. Light-induced gene transfer from packaged DNA enveloped in a dendrimeric photosensitizer. Nat Mater 2005;4:934–41.
25. Jang W-D, Lee C-H, Choi M-S, Osada M. Synthesis of multiporphyrin dendrimer as artificial light-harvesting antennae. J Porphy Phthalocya 2009;13:787–93.
26. Son KJ, Kim S, Kim J-H, et al. Dendrimer porphyrin-terminated polyelectrolyte multilayer micropatterns for a protein microarray with enhanced sensitivity. J Mater Chem 2010;20:6531–8.
27. Sadamoto R, Tomioka N, Aida T. Photoinduced electron transfer reactions through dendrimer architecture. J Am Chem Soc 1996;118:3978–9.
28. Kano K, Fukuda K, Wakami H, et al. Factors influencing self-aggregation tendencies of cationic porphyrins in aqueous solution. J Am Chem Soc 2000;122:7494–502.
29. Shirakawa M, Kawano S, Fujita N, et al. Hydrogen-bond-assisted control of H versus J aggregation mode of porphyrins stacks in an organogel system. J Org Chem 2003;68:5037–44.
30. Maiti NC, Mazumdar S, Periasamy N. J- and H-aggregates of porphyrin-surfactant complexes: time-resolved fluorescence and other spectroscopic studies. J Phys Chem B 1998;102:1528–38.
31. Su WJ, Cooper TM, Brant MC. Investigation of reverse-saturable absorption in brominated porphyrins. Chem Mater 1998;10:1212–13.
32. Obata M, Hirohara S, Tanaka R, et al. In vitro heavy-atom effect of palladium(II) and platinum(II) complexes of pyrrolidine-fused chlorin in photodynamic therapy. J Med Chem 2009;52:2747–53.
33. Tobita S, Arakawa M, Tanaka I. Electronic relaxation processes of rare-earth chelates of benzoyltrifluoroacetone. J Phys Chem 1984;88:2697–702.
34. Tobita S, Arakawa M, Tanaka I. The paramagnetic metal effect on the ligand localized S1-T1 intersystem crossing in the rare-earth-metal complexes with methyl salicylate. J Phys Chem 1985;89:5649–54.
35. Hebbink GA, Grave L, Woldering LA, et al. Unexpected sensitization efficiency of the near-infrared Nd3+, Er3+, and Yb3+ emission by fluorescein compared to eosin and erythrosin. J Phys Chem A 2003;107:2483–91.
36. Klink SI, Grave L, Reinhoudt DN, et al. A systematic study of the photophysical processes in polydentate triphenylene-functionalized Eu^{3+}, Tb^{3+}, Nd^{3+}, Yb^{3+}, and Er^{3+} complexes. J Phys Chem A 2000;104:5457–68.
37. Zorlu Y, Dumoulin F, Durmus M, Ahsen V. Comparative studies of photophysical and photochemical properties of solketal substituted platinum(II) and zinc(II) phthalocyanine sets. Tetrahedron 2010;66:3248–58.
38. Salokhiddinov K, Byteva I, Gurinovich G. Lifetime of singlet oxygen in various solvents. J Appl Spectrosc 1981;34:561–4.